

Demons in the North Atlantic: Variability of deep ocean ventilation

Graeme Alastair MacGilchrist¹, Helen Louise Johnson², Camille Lique³, and David P Marshall²

¹Princeton University

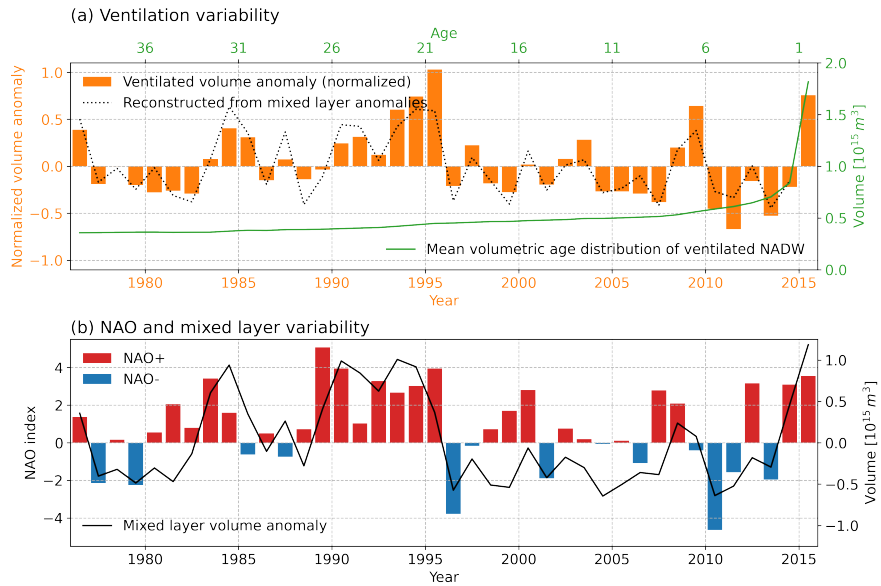
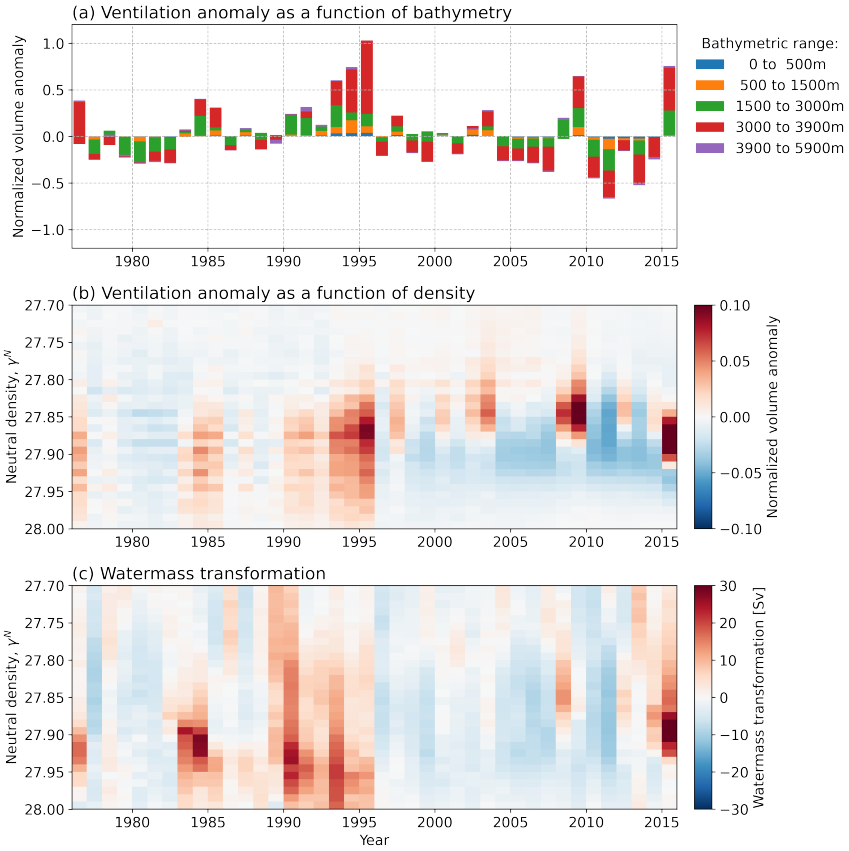
²University of Oxford

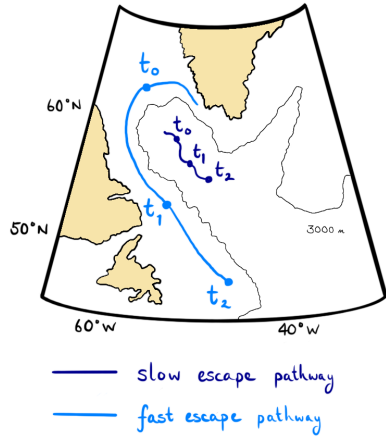
³Laboratoire d’Océanographie Physique et Spatiale

November 23, 2022

Abstract

Translation of atmospheric forcing variability into the ocean interior via ocean ventilation is an important aspect of transient climate change. On a seasonal timescale, this translation is mediated by a so-called ‘Demon’ that prevents access to all except late-winter mixed-layer water. Here, we use an eddy-permitting numerical circulation model to investigate a similar process operating on longer timescales in the high-latitude North Atlantic, which we denote the ‘interannual Demon’. We find that interannual variations in atmospheric forcing are indeed mediated in their translation to the ocean interior. In particular, the signature of persistent strong atmospheric forcing driving deep mixed layers is preferentially ventilated to the interior when the forcing is ceased. Susceptibility to the interannual Demon depends on the location and density of subduction — with the rate at which newly ventilated water escapes its region of subduction being the crucial factor.



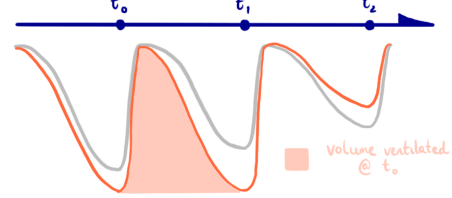


Forcing (NAO)

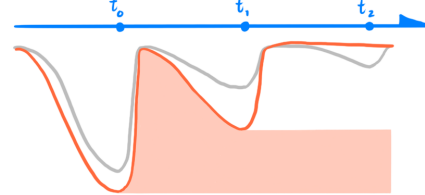


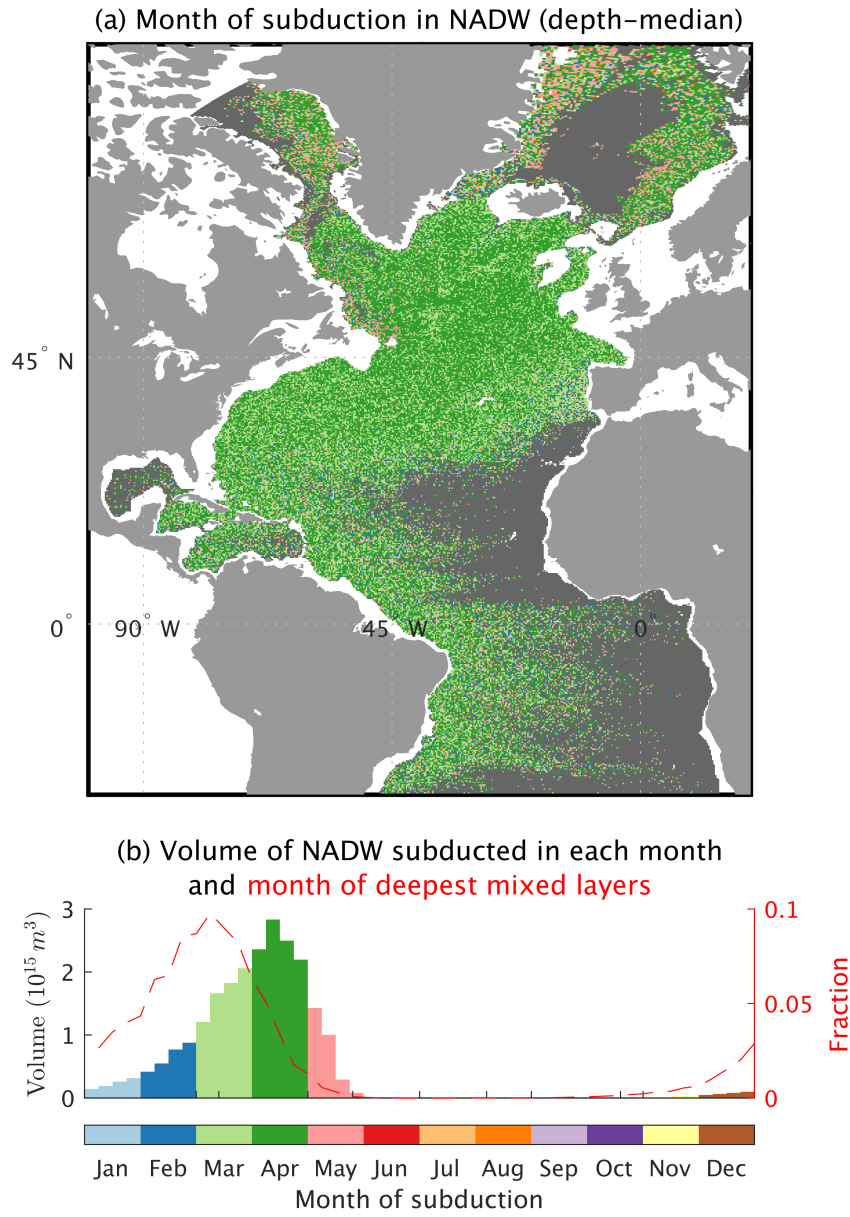
Mixed Layer Depth (following water column)

slow escape (e.g. open ocean)



fast escape (e.g. boundary current)





1 **Demons in the North Atlantic: Variability of deep**
2 **ocean ventilation**

3 **G. A. MacGilchrist¹, H. L. Johnson², C. Lique³, D. P. Marshall⁴**

4 ¹Program in Atmospheric and Oceanic Science, Princeton University, Princeton, N.J., U.S.A.

5 ²Department of Earth Sciences, University of Oxford, Oxford, U.K.

6 ³Univ. Brest, CNRS, IRD, Ifremer, Laboratoire d'Océanographie Physique et Spatiale (LOPS), IUEM,

7 Brest, France

8 ⁴Department of Physics, University of Oxford, Oxford, U.K.

9 **Key Points:**

- 10 • Temporal variability of high-latitude ocean ventilation is investigated using La-
11 grangian trajectories in an eddy-permitting ocean model.
12 • High-latitude ocean ventilation adheres to “Stommel’s Demon”, such that only
13 water subducted in late winter is retained in the subsurface.
14 • An interannual Demon also operates to mediate exchange between the atmosphere
15 and subsurface ocean on longer timescales.

Abstract

Translation of atmospheric forcing variability into the ocean interior via ocean ventilation is an important aspect of transient climate change. On a seasonal timescale, this translation is mediated by a so-called “Demon” that prevents access to all except late-winter mixed-layer water. Here, we use an eddy-permitting numerical circulation model to investigate a similar process operating on longer timescales in the high-latitude North Atlantic, which we denote the “interannual Demon”. We find that interannual variations in atmospheric forcing are indeed mediated in their translation to the ocean interior. In particular, the signature of persistent strong atmospheric forcing driving deep mixed layers is preferentially ventilated to the interior when the forcing is ceased. Susceptibility to the interannual Demon depends on the location and density of subduction — with the rate at which newly ventilated water escapes its region of subduction being the crucial factor.

Plain Language Summary

Water that leaves the ocean’s surface boundary layer — where water is in direct contact with the overlying atmosphere — to be transported into the subsurface, is said to be “ventilated” (the name arising from the abundance of oxygen in newly ventilated water). The ventilation process, which carries implications for the ocean storage of climate-relevant substances such as carbon dioxide, occurs only at certain times and under certain conditions. In describing a mechanism for the selective nature of ventilation over the seasonal cycle, Henry Stommel imagined a Demon sitting at the base of the surface boundary layer, granting access only to parcels of water that meet certain characteristics (namely their speed of “escape”). Thus, “Stommel’s Demon” was born. Here, we investigate this same process as it operates in more northerly regions and on longer timescales. In so doing we give birth to a new “interannual Demon”, and describe its characteristics.

1 Introduction

In 1939, Iselin noted that the properties of the ocean thermocline match those of the late winter mixed layer, as opposed to a year-round average (Iselin, 1939). Some forty years later, Stommel (1979) suggested that this arises from the seasonality of the mixed layer depth, which effectively re-entrains water subducted at any time except late winter. Stommel likened the process to that of “Maxwell’s Demon” in thermodynamics, with the Demon here operating a trapdoor at the base of the mixed layer, allowing access to the ocean interior only for water moving away fast enough to escape re-entrainment. Williams et al. (1995) subsequently used tracers in a numerical simulation to show that this process does indeed operate as Stommel described. The process, which has since become known as “Stommel’s Demon”, allows for the simplification of models of the ocean thermocline, whereby the late-winter mixed layer base can be adopted as the upper boundary and mixed layer seasonality effectively ignored (Luyten et al., 1983; Sarmiento, 1983; Williams, 1991; Qiu & Huang, 1995; D. Marshall & Marshall, 1995; D. Marshall, 1997).

Here, we continue in the Demonic tradition by considering whether a similar process operates on an interannual timescale in the ventilation of deep ocean watermasses, and mediates the translation of atmospheric forcing variability into the ocean subsurface. We focus our attention on the North Atlantic, and in particular on the Labrador Sea, a critical region for the ventilation of the deep waters of the global ocean (Rhein et al., 2017; MacGilchrist et al., 2020). Water subducted here flows southward as part of the Atlantic Meridional Overturning Circulation, returning to the surface predominantly in the Southern Ocean, after a timescale on the order of centuries (DeVries & Primeau, 2011; Gebbie & Huybers, 2012). Consequently, the region has been shown to play a crucial role in transient climate change through the uptake of anthropogenic carbon diox-

66 ide (Khatiwala et al., 2009), oxygen (Koelling et al., 2017), and heat (Zanna et al., 2019).
 67 Understanding the sensitivity of deep ocean ventilation to changes in surface forcing is
 68 thus an important step toward accurately projecting its future evolution (Boer et al., 2007;
 69 Katavouta et al., 2019).

70 The North Atlantic Oscillation (NAO) is the dominant mode of atmospheric vari-
 71 ability over the North Atlantic Ocean (Hurrell, 1995; J. Marshall et al., 2001). Identifi-
 72 fied as an oscillation in the pressure systems over Iceland and the Azores, the system swings
 73 between positive and negative phases on an approximately 3 to 7 year timescale (Hurrell
 74 & Deser, 2010). In its positive phase, the atmospheric circulation is anomalously strong
 75 and stormy, driving enhanced heat loss from the ocean surface across the subpolar gyre
 76 (Visbeck et al., 2003) and resulting in deeper winter mixed layers, particularly in the Labrador
 77 Sea (Sarafanov, 2009; Kieke et al., 2007).

78 In this paper, we consider how, and to what extent, NAO-mediated forcing of the
 79 ocean surface impacts the ventilation of the deep Atlantic Ocean. In particular, we ex-
 80 plore how the interplay of atmospheric forcing and the ocean circulation imparts inter-
 81 annual variability to the transport of mixed layer properties into the ocean subsurface:
 82 an interannual Demon.

83 2 Numerical simulation and Lagrangian trajectory analysis

84 We tackle this problem using trajectory analysis in an eddy-permitting, forced ocean-
 85 sea-ice model. The numerical simulation and Lagrangian trajectory experiments are the
 86 same as those described in MacGilchrist et al. (2020). Here, we summarize the key points
 87 and refer the reader to that previous work for more details, as well as for comparison of
 88 the model with observations in the high-latitude North Atlantic.

89 The numerical simulation is a global implementation of the Nucleus for European
 90 Modelling of the Ocean (NEMO) model (Madec, 2014). The ORCA025 configuration is
 91 used, which has a grid resolution of $1/4^\circ$ (~ 27.75 km at the equator, refined at high lat-
 92 itudes) and 75 uneven vertical levels. The ocean model is coupled to a sea-ice model, LIM2
 93 (Bouillon et al., 2009).

94 The simulation runs from 1958 to 2015, and is forced with the historical atmospheric
 95 reanalysis: ‘Drakkar Forcing Set 5’, which is an updated version of the fields described
 96 in Brodeau et al. (2010). The simulation is initialised from rest with temperature and
 97 salinity from the Levitus climatological hydrography (Levitus et al., 1998). We do not
 98 include the first 18 years of the simulation in our analysis, when the adjustment of the
 99 ocean state to the initial conditions is the largest.

100 Trajectories are evaluated “offline” using the Lagrangian analysis tool, Ariane (Blanke
 101 & Raynaud, 1997). The model velocity and hydrographic fields (output as 5-day means)
 102 are assumed to be piece-wise stationary, changing discretely every 5 days. No attempt
 103 is made to parameterize sub-grid scale physics in the trajectories (van Sebille et al., 2018).
 104 Although the simulation is global, we restrict our Lagrangian experiments to the Atlantic
 105 sector, the extent of which can be seen in Figure 1.

106 We evaluate backwards-in-time trajectories from a model-defined North Atlantic
 107 Deep Water (NADW) with γ^n between 27.7 and 28.0 (see details and discussion in MacGilchrist
 108 et al., 2020), where γ^n is calculated according to the empirical formulation of McDougall
 109 and Jackett (2005). Particles are initialized at each model tracer point (located in the
 110 centre of the grid cell) at the end of September every year between 1976 and 2015. Each
 111 particle is assumed to be representative of the grid-cell volume in which it is initialized.
 112 Trajectories are evaluated backwards in time until reaching the base of the mixed layer,
 113 defined as a neutral density within 0.01 of the density at 10 m, following Thomas et al.
 114 (2015). Our primary results are insensitive to this definition of mixed layer depth.

115 To determine the interannual variability of ventilation, we first calculate the time-
 116 mean age distribution of the model NADW, achieved by averaging the distribution de-
 117 termined for each of the initialization years between 1976 and 2015. Then, we subtract
 118 that mean distribution from the age distribution in 2015, leaving age distribution anomaly
 119 at the end of the simulation. An anomalously large amount of 20 year old water in 2015
 120 signals an anomalously large amount of water retained in the subsurface due to venti-
 121 lation in 1995. We normalize by the mean age distribution to account for re-entrainment
 122 of the watermass over time.

123 3 Results

124 3.1 Stommel’s Demon in NADW

125 Stommel’s Demon was shown to operate in the ventilation of the subtropical ther-
 126 mocline (Williams et al., 1995). However, it is not immediately intuitive that such a pro-
 127 cess operates in the subpolar gyres. In these regions, the time-mean, depth-integrated
 128 flow in the basin interior, away from lateral boundaries, moves water poleward — back
 129 towards the region of deep mixed layers. Furthermore, substantial freshwater input (from
 130 glacial and sea-ice melt, as well as river run-off from the Arctic) and deep convective events
 131 combine to ensure that isopycnal outcrop migration does not occur in a strictly merid-
 132 ional fashion. Consequently, water subducted into NADW in summer could feasibly evade
 133 re-entrainment, dependent on its subsurface pathway (*e.g.* transported southward in the
 134 western boundary current).

135 The month in which ventilated NADW is subducted from the mixed layer is shown
 136 in Figure 1. In panel (a) we show the month of subduction in each grid cell, averaged
 137 over the depth of NADW. The dominance of light and dark green illustrates that the ma-
 138 jority of ventilation arises from subduction occurring in March and April, confirmed by
 139 the volumetric histogram in panel (b), and revealing that, as noted by Williams et al.
 140 (1995) for the subtropics, Stommel’s Demon functions similarly in the high-latitudes. The
 141 histogram further shows that, although the peak is in late winter, ventilation of NADW
 142 takes place over a broad range of winter months, from December through May.

143 The dashed line in Figure 1b shows a probability distribution for the timing of the
 144 deepest mixed layers across the high-latitude North Atlantic domain. Throughout the
 145 year there is a strikingly consistent lag of approximately one month between the tim-
 146 ing of deepest mixed layers and that of subduction. MacGilchrist et al. (2020) noted that
 147 the majority of NADW ventilation occurs via subduction over a relatively narrow region
 148 in the Labrador Sea boundary current. In this region, the deepest mixed layers occur
 149 slightly later in the year than they do in the open ocean subpolar gyre, perhaps explain-
 150 ing part of the shift between the two curves in Figure 1b and emphasizing that the *lo-*
 151 *cation* of subduction is a crucial component of ventilation, in addition to the timing.

152 3.2 An interannual Demon

153 The normalized anomaly in the age distribution of NADW, which we adopt as a
 154 proxy for ventilation variability (see Section 2), is shown in Figure 2a (orange bars). The
 155 time-mean age distribution is also shown (green line), for which we can note the long-
 156 timescale decline in volume with increasing age, indicative of a slow erosion of the wa-
 157 termass as it is mixed diabatically or returned to the mixed layer. The interannual sig-
 158 nal is strong, varying by as much as 100% of the mean (a normalized anomaly value of
 159 1).

160 We wish to understand how variability in ventilation is related to atmospheric forc-
 161 ing of the upper ocean. In panel (b), we show the NAO index from Hurrell (1995, red
 162 and blue bars) as well as the anomaly in the integrated volume of the mixed layer. As

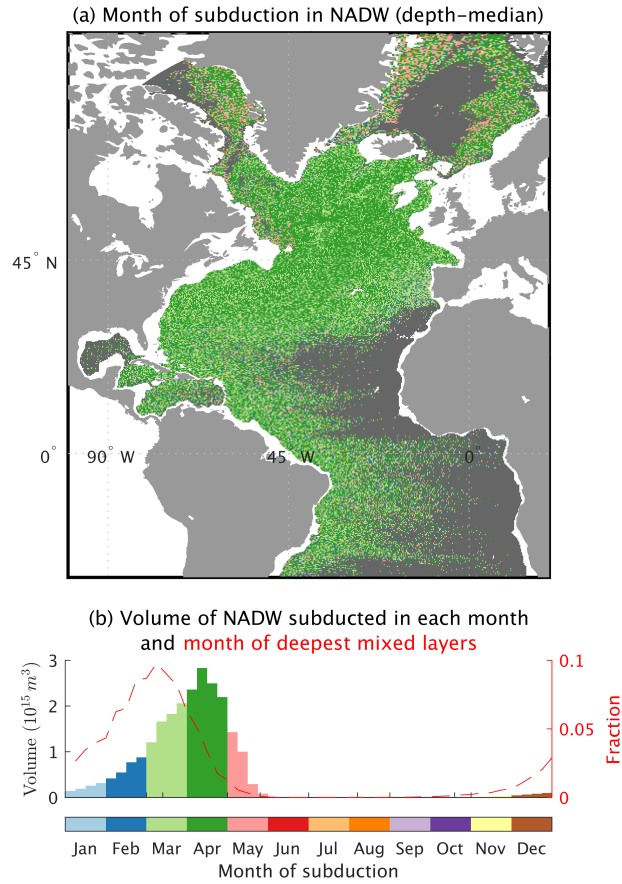


Figure 1. (a) Depth-median month of subduction for ventilated NADW in 2015. Dark gray indicates regions unventilated during the simulation. (b) Distribution of the month of subduction (colored bars; volumetric distribution derived from trajectories) and the month of deepest mixed layers (red dashed line; distribution of surface area fraction derived from the Eulerian fields). The dashed curve is evaluated by first determining the timing of the deepest mixed layer over the course of each year for each grid cell in the high-latitude North Atlantic (North of $40^\circ N$). A histogram is taken over all years and across all grid cells and the surface area occupied by each month is divided by the total surface area. Thus, the fraction denotes the probability that, for a given location and a given year, the deepest mixed layer occurred during that month.

163 expected (Visbeck et al., 2003), these two are well-correlated, indicating that changes
 164 in the atmospheric state have an impact on the depth of the upper ocean mixed layer.

165 Some variability in atmospheric forcing (Figure 2b) is translated to the ventilation
 166 anomalies (Figure 2a), at least in the sense that broad periods of positive NAO appear
 167 to match times of anomalously large ventilation (*e.g.* the 1990s). However, it is evident
 168 that the ventilation anomalies do not entirely match up with anomalies in the atmospheric
 169 state or upper ocean. This suggests that ventilation variability is also mediated by up-
 170 per ocean dynamics.

171 Linear regression reveals that, as anticipated from Figure 2b, the volume of water
 172 present in the mixed layer in each year is well-correlated with the NAO ($R^2 = 0.41$).
 173 However, that correlation is eroded (to $R^2 = 0.14$) when considering only the amount
 174 of that water left in the subsurface following re-entrainment in the subsequent winter.
 175 In contrast, correlation between the final ventilation anomaly (Figure 2a) and the vol-
 176 ume subducted each year is improved following re-entrainment (from $R^2 = 0.61$ to $R^2 =$
 177 0.85). Such correlations show that while ventilation anomalies are initially established
 178 by atmospheric forcing variability, they are confounded by variations in the re-entrainment
 179 of water from year-to-year. That is, an interannual Demon mediates the years in which
 180 atmospheric forcing anomalies are “felt” by the deep ocean.

181 Of course, the deep mixed layers in any given year and the re-entrainment in the
 182 following year are *both* a result of atmospheric forcing, since re-entrainment itself is de-
 183 pendent on the subsequent year’s mixed layer depth (with deeper mixed layers entrain-
 184 ing more water). What is apparent here is that ventilation anomalies have a *memory* of
 185 at least 2 years of atmospheric forcing, manifest in the varying depth of the winter mixed
 186 layer. The dotted line in Figure 2a is a reconstruction of the ventilation anomaly based
 187 on mixed layer depth anomalies in each year and in the subsequent year; that is, rep-
 188 resenting ventilation as a forwards-in-time AR1 process. The reconstruction does a rea-
 189 sonable job in most years, and we find that the cumulative error is approximately halved
 190 compared to an equivalent reconstruction for an AR0 process (ventilation anomaly de-
 191 pendent only on the mixed layer depth anomaly in each year). Failing to account for the
 192 time-varying deep winter mixed layer thus results in the accumulation of errors in es-
 193 timating ventilation to the ocean interior.

194 Two time periods (the early 1990s and late 2000s) provide particularly clear ex-
 195 amples of the mediation of ventilation by atmospheric forcing variability. During the 1990s,
 196 there was a consistently strong, positive NAO, accompanied by deep winter mixed lay-
 197 ers (Figure 2b). However, substantial positive ventilation anomalies are only present in
 198 the later years (Figure 2a), after 1993, and largest in the final year (1995), just before
 199 the NAO moved back into a negative phase. Likewise in 2008 and 2009, the ventilation
 200 anomaly peaks in the year following the transition to a negative NAO.

201 3.3 Deep convection and the open-ocean Demon

202 MacGilchrist et al. (2020) note that almost all of the ventilation in this simulation
 203 occurs in the boundary current of the Labrador Sea. We might question then, whether
 204 it is also in this region that the Demon operates, or whether the signal arises from deep
 205 convection in the central Labrador Sea.

206 Figure 3a shows the ventilation anomaly (as in Figure 2a) now separated by the
 207 bathymetric depth in the region where the particles left the mixed layer — as a proxy
 208 for whether the subduction occurred in the boundary current (shallower than 3000 m bathy-
 209 metric depth) or in the open ocean (deeper than 3000 m bathymetric depth). Anoma-
 210 lies associated with subduction in the boundary current make a broadly consistent con-
 211 tribution over time. On the other hand, major excursions are the result of anomalies in

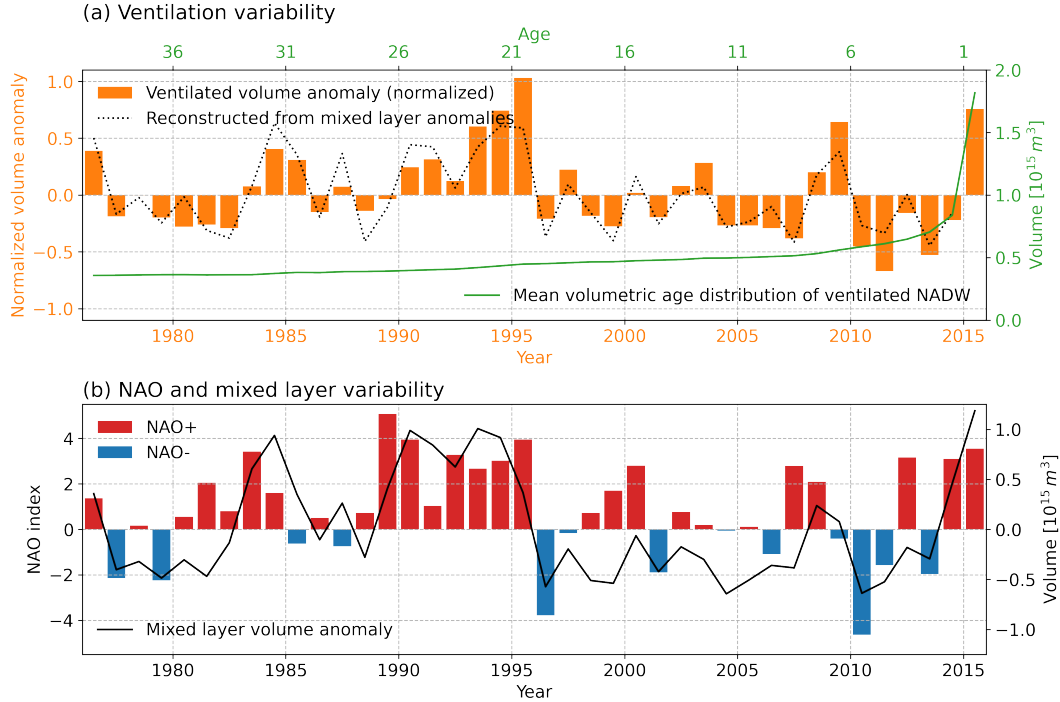


Figure 2. (a) Ventilation variability, as derived from the Lagrangian experiments. Green line is the mean age distribution of NADW from a number of different initialization years (see Section 2). Orange bars are the normalized anomaly around this mean age distribution for the initialization in 2015, which we take as a proxy for the ventilation anomaly in each year (*e.g.* + anomaly in 20 year old water implies + anomaly in 1995 ventilation, etc.). The dotted line is a reconstruction of the ventilation anomaly using multi-linear regression of mixed layer anomalies in the year itself and in the following year. (b) Atmospheric forcing and upper ocean response. Red and blue bars are the DJFM NAO index from Hurrell (1995). The solid line is the anomaly in the volume of the late winter mean mixed layer (*i.e.*, the volume of water that is within 0.01 of the surface density above it).

212 the open ocean, particularly forming the dominant contribution to the large anomalies
 213 in the 1990s.

214 A similar picture emerges when we consider the density class in which the venti-
 215 lation anomalies appear. Figure 3b again shows the ventilation anomaly from Figure 2,
 216 here split by the density of the water at the end of the simulation. Anomalies prior to
 217 the mid-1990s appear in the densest density classes, and latterly shift towards mid-range
 218 and lighter densities. As noted in MacGilchrist et al. (2020), denser waters are prefer-
 219 entially subducted in the central Labrador Sea. Anomalies in the densest water masses
 220 are crucial in establishing the large positive deviations in the early part of the time-series
 221 and negative anomalies thereafter, interspersed with large positive anomalies in the in-
 222 termediate classes. This apparent shift in the ventilation of the densest water masses is
 223 consistent with observed changes in the central Labrador Sea, for which the mid-1990s
 224 marked a shift in the formation of Labrador Sea Water (Kieke et al., 2007).

225 To return again to the relation between ventilation and surface forcing variability,
 226 we consider the surface-forced watermass transformation (Walín, 1982; Groeskamp et
 227 al., 2019). This is evaluated as the divergence of the integrated surface density flux within

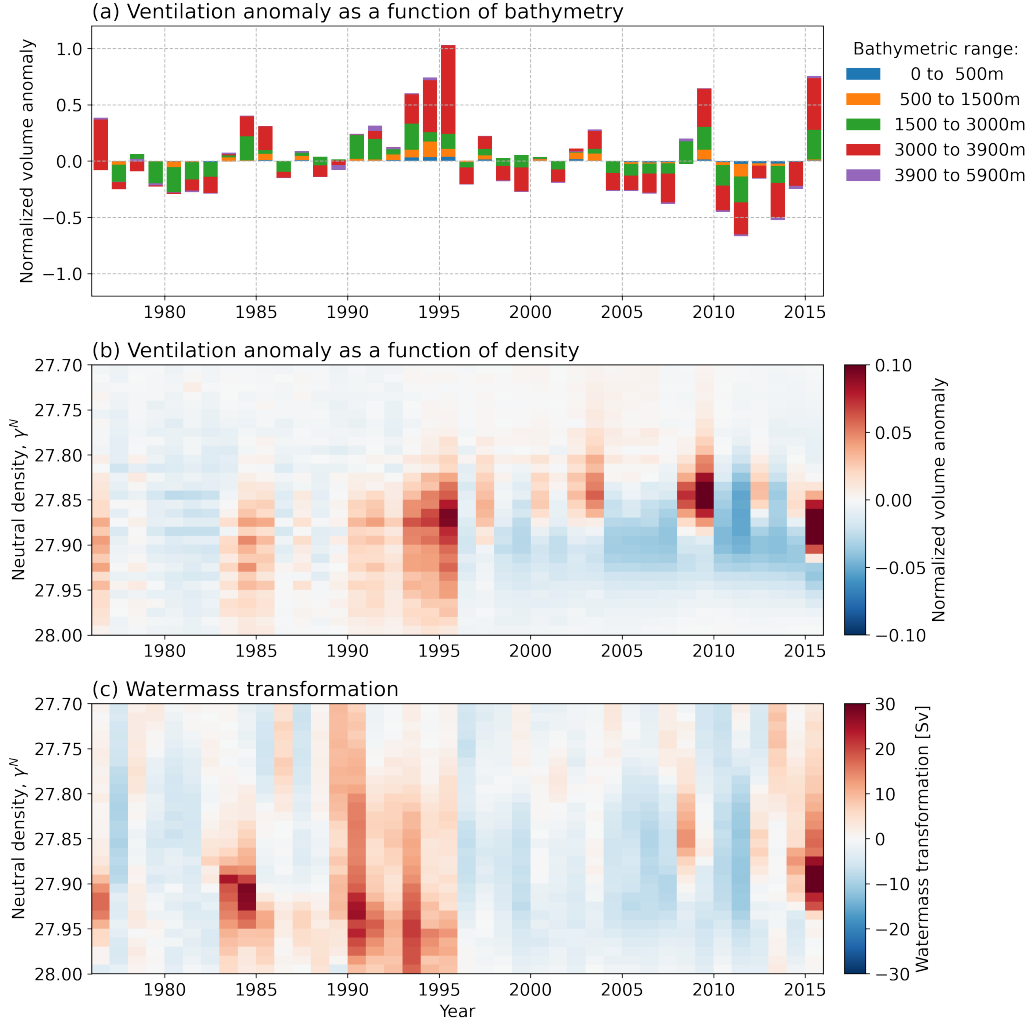


Figure 3. (a) Normalized ventilation anomaly (as in Figure 2a) separated according to the bathymetric contour over which subduction took place. (b) Normalized ventilation anomaly as a function of the neutral density of the water in September 2015 (simulation end). (c) Surface watermass transformation anomaly as a function of neutral density.

228 density bins of width $\Delta\gamma^n = 0.01$ across the North Atlantic domain, and reveals the
 229 transport of water across each density contour due to surface buoyancy forcing. We see
 230 in Figure 3c that the surface-forced transformation exhibits variability that is broadly
 231 consistent with that of ventilation, particularly on a time-scale consistent with that of
 232 the NAO (Figure 2). Noting again that the ventilation anomalies are evaluated only from
 233 the Lagrangian pathways of the model, it is striking that they should exhibit such clear
 234 memory of the surface forcing even to the end of the simulation and in the presence of
 235 the substantial subsurface mixing MacGilchrist et al. (2020). Closer consideration of Fig-
 236 ure 3 reveals that ventilation anomalies exhibit deviations from variability imparted purely
 237 by the surface forcing, consistent with our impression from Figure 2. Maxima in ven-
 238 tilation in each density class arise *after* periods of sustained transformation anomalies
 239 (see, for example, the mid-1980s, mid-1990s and late 2000s), indicative of the interan-
 240 nual Demon at work.

4 Conclusions

Ventilation of the deep Atlantic occurs in late winter (Figure 1) and exhibits substantial variability on interannual and longer time-scales (Figure 2). Variability in atmospheric forcing associated with the NAO imparts a multi-annual (3- to 7-year) time-scale on ocean ventilation through its impact on mixed layer depth. However, variations in the fraction of water that is re-entrained each year imparts an additional signature on the subsurface ocean (Figures 2 and 3). That is, water from particular years, selected for by changes in the depth of the late-winter mixed-layer and the pace of escape from the subduction location, preferentially ventilates the deep Atlantic: a process we call the “interannual Demon” by analogy with Stommel’s 1979 paper on the seasonal Demon.

We illustrate the operation of the interannual Demon in Figure 4. Borrowing from schematic representations of Williams et al. (1995), we follow the Lagrangian evolution of water columns as they move progressively away from, or “escape”, regions of deepest mixed layers. We consider two regimes: one in which that escape is slow and one in which it is fast; manifest in the extent to which the winter mixed layer shallows year-on-year under constant forcing conditions (gray lines). As an illustrative example, we consider variable interannual forcing (red lines) consisting of two years of progressively more positive NAO followed by a year of negative NAO. Along the slow escape pathway, the deepening of the mixed layer associated with the second year of positive NAO exceeds the natural shoaling of the mixed layer due to the water column’s lateral displacement. Consequently, all of the water that leaves the mixed layer after the first winter is re-entrained the following year. No signature of ventilation from the first year is thus retained in the ocean subsurface, despite the positive NAO anomaly and deeper-than-normal mixed layer in that year. In this way, we can see how interannual variability mediates the passage of water into the subsurface ocean. In contrast, along the fast escape pathway, the natural shoaling of the mixed layer far exceeds the forcing-derived deepening of the winter mixed layer in the second year, allowing water subducted in the first year to remain in the subsurface. Thus, the pathway of newly ventilated water is a critical determinant for the influence of atmospheric variability and the operation of an interannual Demon.

As well as illustrating the impact of a time-varying mixed layer depth on ocean ventilation, the interannual demon has important practical implications. In particular, it is common to adopt the late-winter mixed layer depth and its year-to-year variation as a proxy for ocean ventilation and its variability (Boe et al., 2009; Li et al., 2016; Heuz, 2017). That perspective ignores the impact of an interannual Demon mediating the translation of surface variability into the subsurface ocean. We noted in Section 3.2 that this leads to a cumulative error in the estimation of ventilated volume. More appropriate, at least in this case for the North Atlantic, is to construct a model for ventilation that incorporates interannual changes in late-winter mixed layer depth (Figure 2a).

Although we have focused our analysis on the high-latitude North Atlantic, the interannual Demon could be operating across the global ocean. Based on our analysis, it is likely to be operating where the year-on-year changes in winter mixed layer depth exceed, or come close to, the change of the mean winter mixed layer depth over the lateral annual displacement of the fluid column (Figure 4). In the case of the North Atlantic, this is intricately connected to the occurrence of deep convection and the cyclonic circulation within the open-ocean Labrador Sea. Other potential locations then include the high-latitude Southern Ocean where convective events are thought to occur only sporadically (Killworth, 1983; Bernardello et al., 2014). Alternatively, mode and intermediate waters in the Southern Ocean, whose formation regions display substantial year-on-year variability in mixed layer depth and formation volume (Kolodziejczyk & Llovel, 2019; Qu et al., 2020), might also be good candidates for the operation of an interannual Demon.

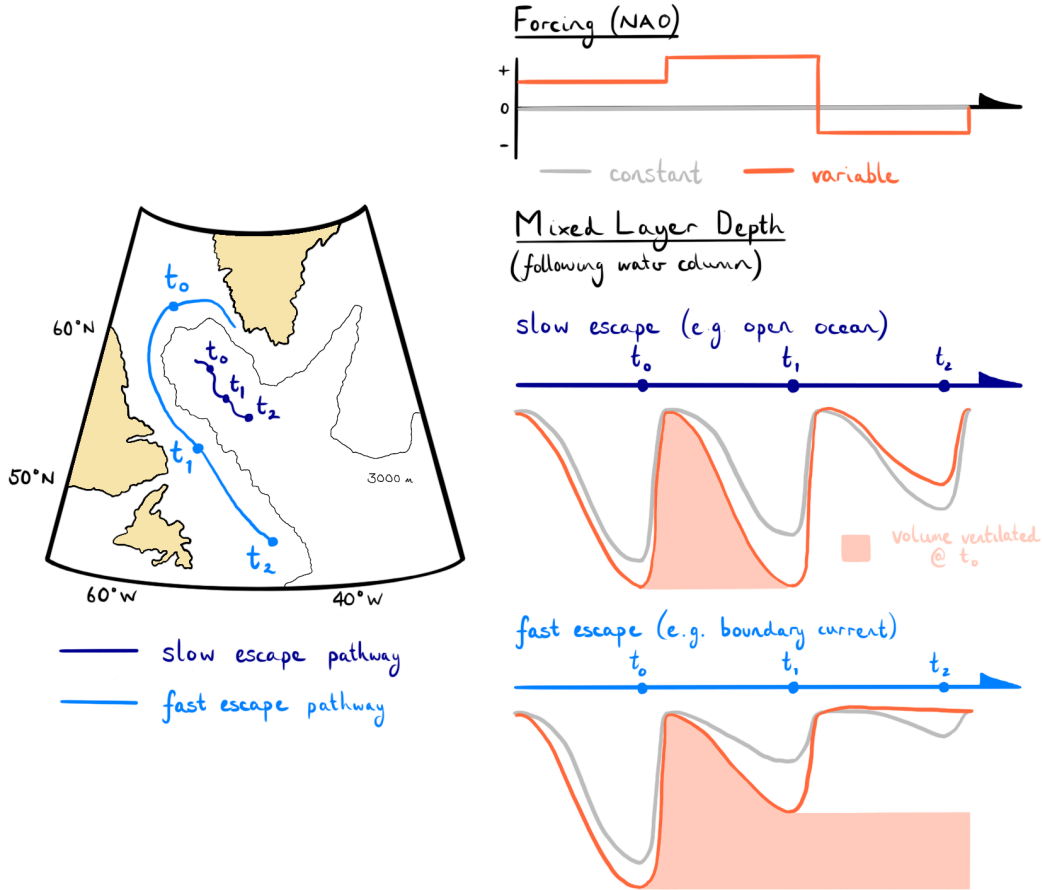


Figure 4. Schematic illustration of the operation of an interannual Demon, and the dependence on the speed at which newly subducted water moves away from the region of deep mixed layers and hence evades re-entrainment. On the left, we show two idealized pathways of water columns exiting the Labrador Sea. One pathway corresponds to transport in the central, open-ocean region (dark blue), while the other corresponds to transport via the boundary current (light blue). The positions of the columns in late winter of successive years are labeled t_i . On the right, we show the corresponding evolution of the mixed layer depth following these two water columns under constant forcing (gray lines) and variable forcing (red lines). The pattern of these forcings is shown on the top right, represented as idealized variations of the NAO. For the variable forcing case, we keep track of the water ventilated during the first winter (t_0), represented by the pink patch.

293 Finally, we have noted that the interannual Demon operates effectively in the open-
 294 ocean Labrador Sea because water there escapes only slowly and thus is frequently re-
 295 turned to the mixed layer. Such persistent re-ventilation, however, could actually increase
 296 the uptake and sequestration of certain atmospheric tracers. Carbon dioxide has a long
 297 equilibration timescale (between 6 and 18 months Jones et al., 2014) meaning that max-
 298 imal exchange between the atmosphere and ocean requires water to be exposed to the
 299 atmosphere for more than a year. The interannual Demon might thus enhance the up-
 300 take of carbon in the open ocean Labrador Sea, since waters that eventually permanently
 301 subduct are likely to have had more time to reach equilibrium. It could thus be the case
 302 that the Demon is partly responsible for establishing the location and efficiency of an-
 303 thropogenic carbon uptake.

304 Acronyms

305 **NADW** North Atlantic Deep Water

306 Acknowledgments

307 Code for reproducing the figures presented here is available on GitHub (github.com/gmacgilchrist;
 308 in repositories ‘nadw’ for Figure 1 and ‘draw_figs_nadw’ for Figures 2 and 3). The NEMO
 309 Ocean Model core is available at <https://forge.ipsl.jussieu.fr/nemo/chrome/site/doc/NEMO/guide/html/install.html>.
 310 The Lagrangian trajectory calculation software, Ariane, is available at [https://stockage.univ-](https://stockage.univ-brest.fr/grima/Ariane/)
 311 [brest.fr/ grima/Ariane/](https://stockage.univ-brest.fr/grima/Ariane/). Model output used in this study can be obtained upon request
 312 to CL (camille.lique@ifremer.fr). GM is supported through NSF’s Southern Ocean Car-
 313 bon and Climate Observations and Modeling (SOCCOM) Project under the NSF Award
 314 PLR-1425989, with additional support from NOAA and NASA. HJ and DM were sup-
 315 ported by the UK Natural Environment Research Council OSNAP project (NE/K010948/1).
 316 CL was supported by the project MEDLEY funded by JPI Climate and JPI Oceans. The
 317 hindcast was carried out within the European Drakkar project, and the model outputs
 318 were kindly provided by J.M Molines and C. Talandier. We used the computational tool
 319 Ariane developed by B. Blanke and N. Grima, who also provided support and advice on
 320 its use.

321 References

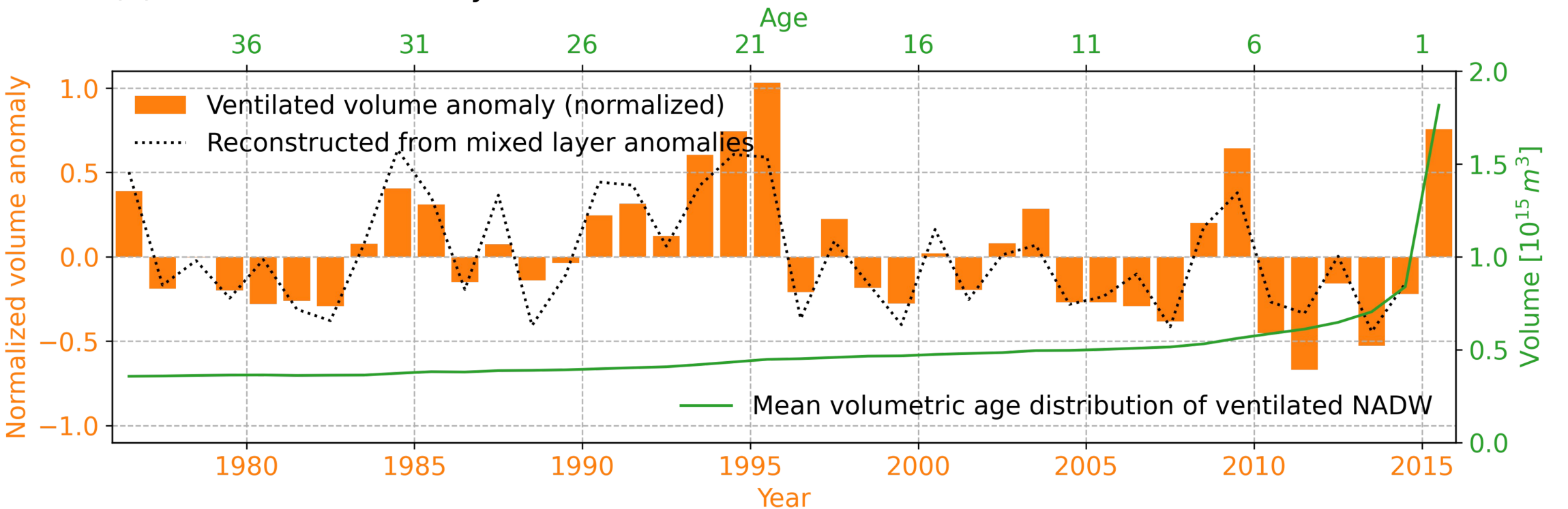
- 322 Bernardello, R., Marinov, I., & Palter, J. (2014). Impact of weddell sea deep convec-
 323 tion on natural and anthropogenic carbon in a climate model. *Geophysical*.
 324 Blanke, B., & Raynaud, S. (1997). Kinematics of the pacific equatorial undercur-
 325 rent: An eulerian and lagrangian approach from gcm results. *Journal of Physi-*
 326 *cal Oceanography*, 27(6), 10381053.
 327 Boer, A. D., Sigman, D., & Toggweiler, J. (2007). Effect of global ocean temperature
 328 change on deep ocean ventilation. .
 329 Bouillon, S., Morales Maqueda, M. A., Legat, V., & Fichet, T. (2009). An elastic-
 330 viscous-plastic sea ice model formulated on arakawa b and c grids. *Ocean Mod-*
 331 *elling*, 27(3-4), 174184.
 332 Boe, J., Hall, A., & Qu, X. (2009). Deep ocean heat uptake as a major source of
 333 spread in transient climate change simulations. *Geophysical Research Letters*,
 334 36(22), 15.
 335 Brodeau, L., Barnier, B., Treguier, A. M., Penduff, T., & Gulev, S. (2010). An
 336 era40-based atmospheric forcing for global ocean circulation models. *Ocean*
 337 *Modelling*, 31(3-4), 88104.
 338 DeVries, T., & Primeau, F. (2011). Dynamically and observationally constrained
 339 estimates of water-mass distributions and ages in the global ocean. *Journal of*
 340 *Physical Oceanography*, 41(12), 23812401.

- 341 Gebbie, G., & Huybers, P. (2012). The mean age of ocean waters inferred from
 342 radiocarbon observations: Sensitivity to surface sources and accounting for
 343 mixing histories. *Journal of Physical Oceanography*, *42*(2), 291305.
- 344 Groeskamp, S., Griffies, S., & Iudicone, D. (2019). The water mass transformation
 345 framework for ocean physics and biogeochemistry. *Annual review of*.
- 346 Heuz, C. (2017). North atlantic deep water formation and amoc in cmip5 models.
 347 *Ocean Science*.
- 348 Hurrell, J. W. (1995). Decadal trends in the north atlantic oscillation: regional tem-
 349 peratures and precipitation. *Science*, *269*(5224), 676679.
- 350 Hurrell, J. W., & Deser, C. (2010). North atlantic climate variability: the role of the
 351 north atlantic oscillation. *Journal of marine systems*, *79*(3-4), 231244.
- 352 Iselin, C. O. (1939). The influence of vertical and lateral turbulence on the charac-
 353 teristics of the waters at mid-depths. *Eos, Transactions American Geophysical*
 354 *Union*, *20*(3), 414417.
- 355 Jones, D., Ito, T., & Takano, Y. (2014). Spatial and seasonal variability of the air-
 356 sea equilibration timescale of carbon dioxide. *Global Biogeochemical*.
- 357 Katavouta, A., Williams, R., & Goodwin, P. (2019). The effect of ocean ventilation
 358 on the transient climate response to emissions. *Journal of Climate*.
- 359 Khatiwala, S., Primeau, F., & Hall, T. (2009). Reconstruction of the history of an-
 360 thropogenic co₂ concentrations in the ocean. *Nature*, *462*(7271), 346349.
- 361 Kieke, D., Rhein, M., Stramma, L., Smethie, W. M., Bullister, J. L., & LeBel, D. A.
 362 (2007). Changes in the pool of labrador sea water in the subpolar north at-
 363 lantic. *Geophysical Research Letters*, *34*(6).
- 364 Killworth, P. (1983). Deep convection in the world ocean. *Reviews of Geophysics*.
- 365 Koelling, J., Wallace, D. W., Send, U., & Karstensen, J. (2017). Intense oceanic
 366 uptake of oxygen during 20142015 winter convection in the labrador sea. *Geo-*
 367 *physical Research Letters*, *44*(15), 78557864.
- 368 Kolodziejczyk, N., & Llovel, W. (2019). Interannual variability of upper ocean water
 369 masses as inferred from argo array. *Journal of Geophysical*.
- 370 Levitus, S., Boyer, T., Conkright, M., Brien, T. O., Antonov, J., Stephens, C., ...
 371 Gelfeld, R. (1998). *Noaa atlas nesdis 18, world ocean database 1998*. Washing-
 372 ton D.C.: U.S. Government Printing Office.
- 373 Li, H., Ilyina, T., Mller, W., & Sienz, F. (2016). Decadal predictions of the north at-
 374 lantic co₂ uptake. *Nature communications*.
- 375 Luyten, J., Pedlosky, J., & Stommel, H. (1983). The ventilated thermocline. *Journal*
 376 *of Physical Oceanography*, *13*(2), 292309.
- 377 MacGilchrist, G., Johnson, H., & Marshall, D. (2020). Locations and mechanisms
 378 of ocean ventilation in the high-latitude north atlantic in an eddy-permitting
 379 ocean model. *Journal of*.
- 380 Madec, G. (2014). *Nemo ocean engine*. Note du Pole de modelisation de lInstitut
 381 Pierre-Simon Laplace No 27.
- 382 Marshall, D. (1997). Subduction of water masses in an eddying ocean. *Journal of*
 383 *Marine Research*, *55*(2), 201222.
- 384 Marshall, D., & Marshall, J. (1995). On the thermodynamics of subduction. *Journal*
 385 *of physical oceanography*, *25*(1), 138151.
- 386 Marshall, J., Johnson, H., & Goodman, J. (2001). A study of the interaction of
 387 the north atlantic oscillation with ocean circulation. *Journal of Climate*, *14*(7),
 388 13991421.
- 389 McDougall, T. J., & Jackett, D. R. (2005). The material derivative of neutral den-
 390 sity. *Journal of Marine Research*, *63*, 159185.
- 391 Qiu, B., & Huang, R. X. (1995). Ventilation of the north atlantic and north pa-
 392 cific: subduction versus obduction. *Journal of Physical Oceanography*, *25*(10),
 393 23742390.
- 394 Qu, T., Gao, S., & Fine, R. (2020). Variability of the sub-antarctic mode water sub-
 395 duction rate during the argo period. *Geophysical Research Letters*.

- 396 Rhein, M., Steinfeldt, R., Kieke, D., Stendardo, I., & Yashayaev, I. (2017). Venti-
397 lation variability of labrador sea water and its impact on oxygen and anthro-
398 pogenic carbon: a review. *Philosophical Transactions of the Royal Society A:
399 Mathematical, Physical and Engineering Sciences*, *375*(2102), 20160321.
- 400 Sarafanov, A. (2009). On the effect of the north atlantic oscillation on temperature
401 and salinity of the subpolar north atlantic intermediate and deep waters. *ICES
402 Journal of Marine Science*, *66*(7), 14481454.
- 403 Sarmiento, J. (1983). A tritium box model of the north atlantic thermocline. *Jour-
404 nal of Physical Oceanography*, *13*(7), 12691274.
- 405 Stommel, H. (1979). Determination of water mass properties of water pumped
406 down from the ekman layer to the geostrophic flow below. *Proceedings of the
407 National Academy of Sciences*, *76*(7), 30513055.
- 408 Thomas, M. D., Treguier, A.-m., Blanke, B., Deshayes, J., & Voltaire, A. (2015).
409 A lagrangian method to isolate the impacts of mixed layer subduction on the
410 meridional overturning circulation in a numerical model. *Journal of Climate*,
411 *28*, 75037517.
- 412 van Sebille, E., Griffies, S. M., Abernathey, R. P., Adams, T. P., Berlo, P., Biastoch,
413 A., ... Zika, J. D. (2018). Lagrangian ocean analysis : Fundamentals and
414 practices. *Ocean Modelling*, *121*, 4975.
- 415 Visbeck, M., Chassignet, E. P., Curry, R. G., Delworth, T. L., Dickson, R. R., &
416 Krahnemann, G. (2003). The oceans response to north atlantic oscillation
417 variability. In *The north atlantic oscillation: Climatic significance and environ-
418 mental impact* (p. 113-146). American Geophysical Union.
- 419 Walin, G. (1982). On the relation between sea-surface heat flow and thermal circula-
420 tion in the ocean. *Tellus*, *34*(2), 187195.
- 421 Williams, R. G. (1991). The role of the mixed layer in setting the potential vorticity
422 of the main thermocline. *Journal of Physical Oceanography*, *21*(12), 18031814.
- 423 Williams, R. G., Marshall, J. C., & Spall, M. A. (1995). Does stommels mixed layer
424 demon work. *Journal of Physical Oceanography*, *25*(12), 30893102.
- 425 Zanna, L., Khatiwala, S., Gregory, J. M., Ison, J., & Heimbach, P. (2019). Global re-
426 construction of historical ocean heat storage and transport. *Proceedings of the
427 National Academy of Sciences*, *116*(4), 11261131.

Figure 2.

(a) Ventilation variability



(b) NAO and mixed layer variability

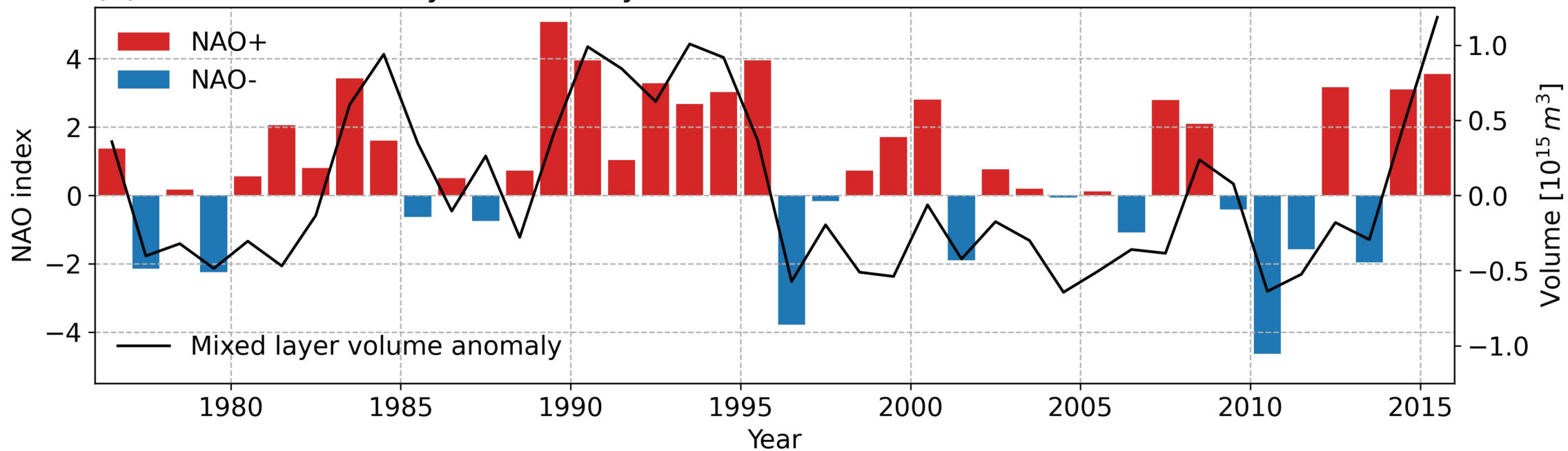
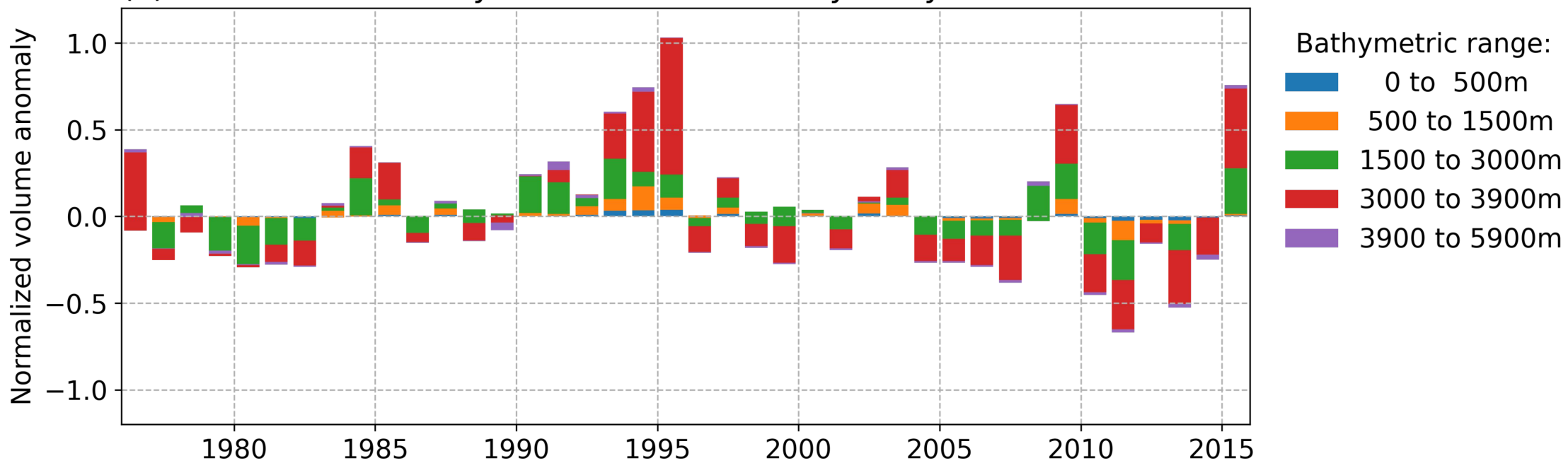
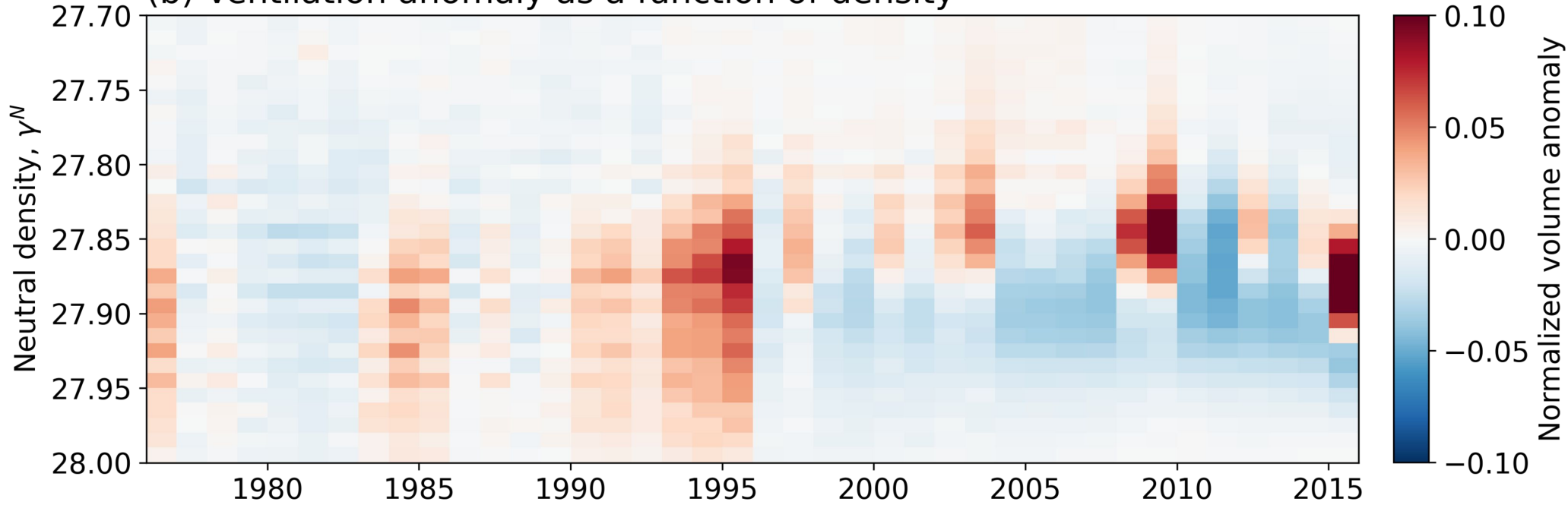


Figure 3.

(a) Ventilation anomaly as a function of bathymetry



(b) Ventilation anomaly as a function of density



(c) Watermass transformation

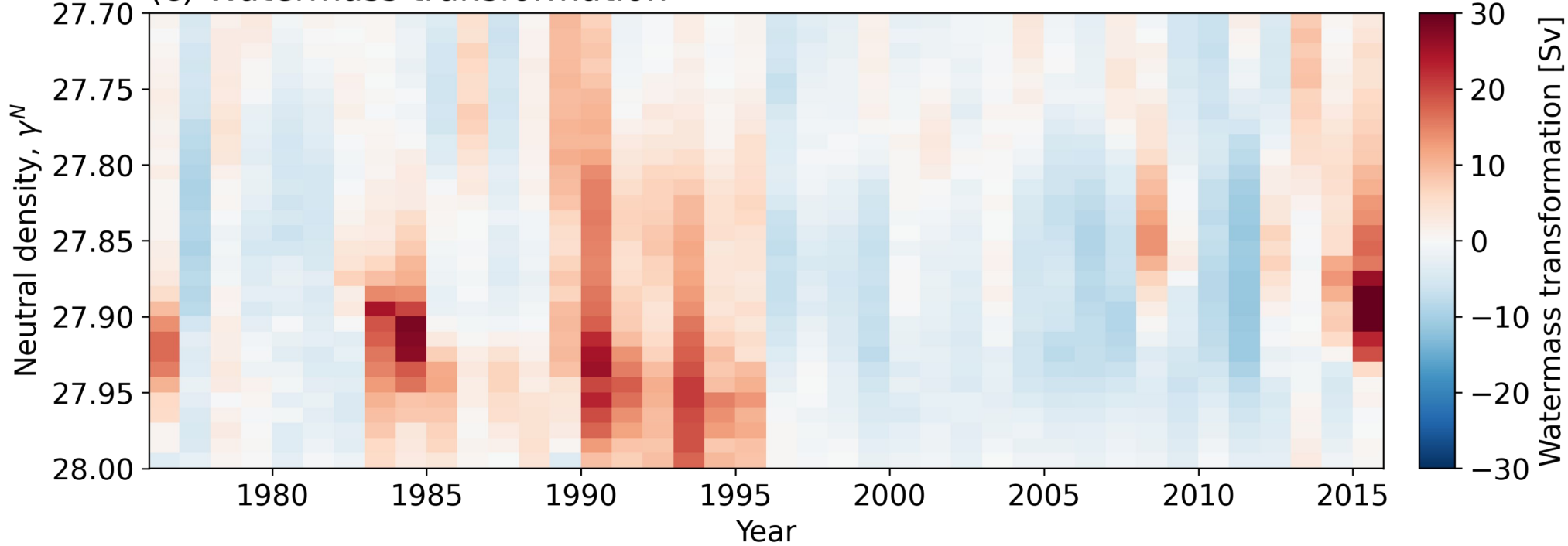
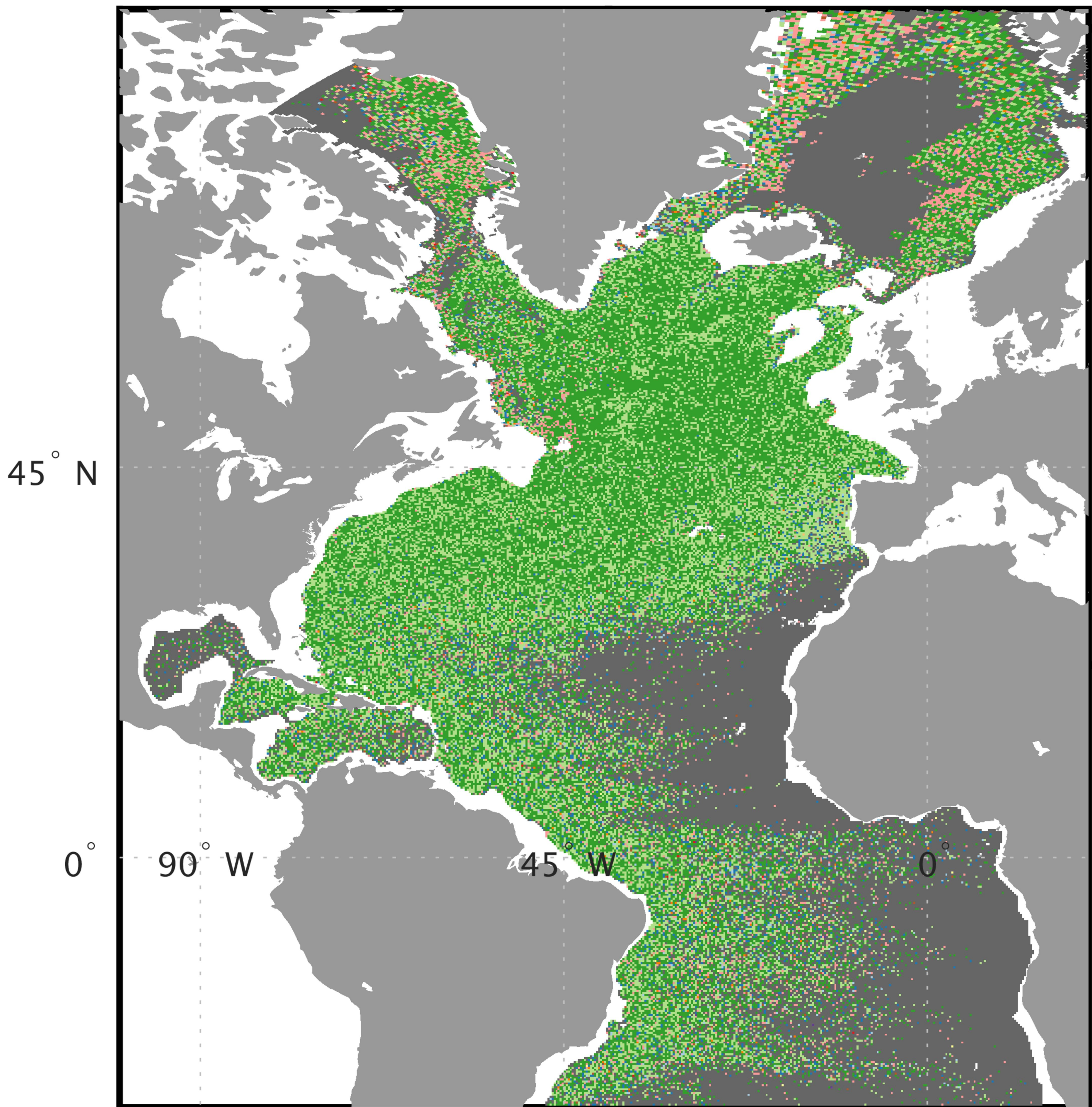


Figure 1.

(a) Month of subduction in NADW (depth–median)



(b) Volume of NADW subducted in each month and **month of deepest mixed layers**

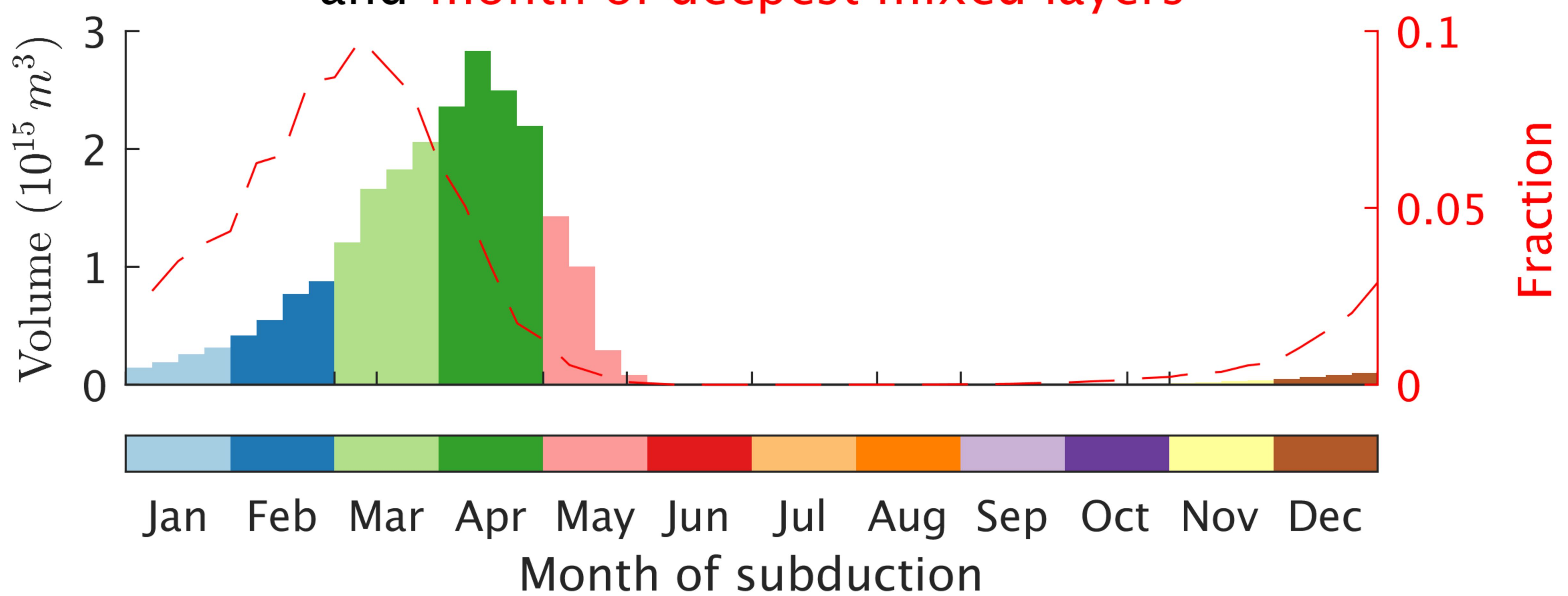
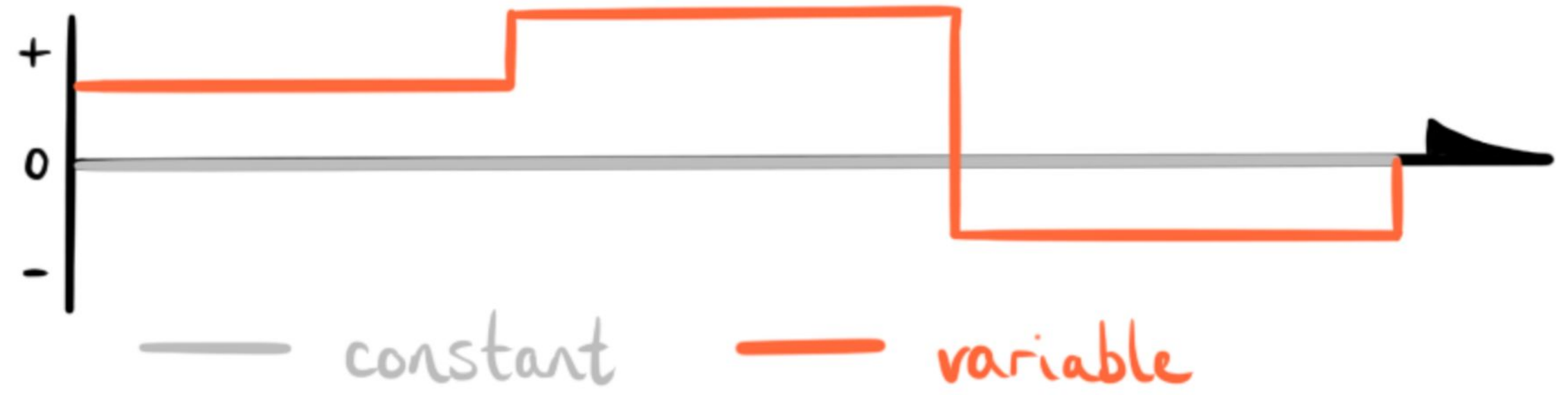


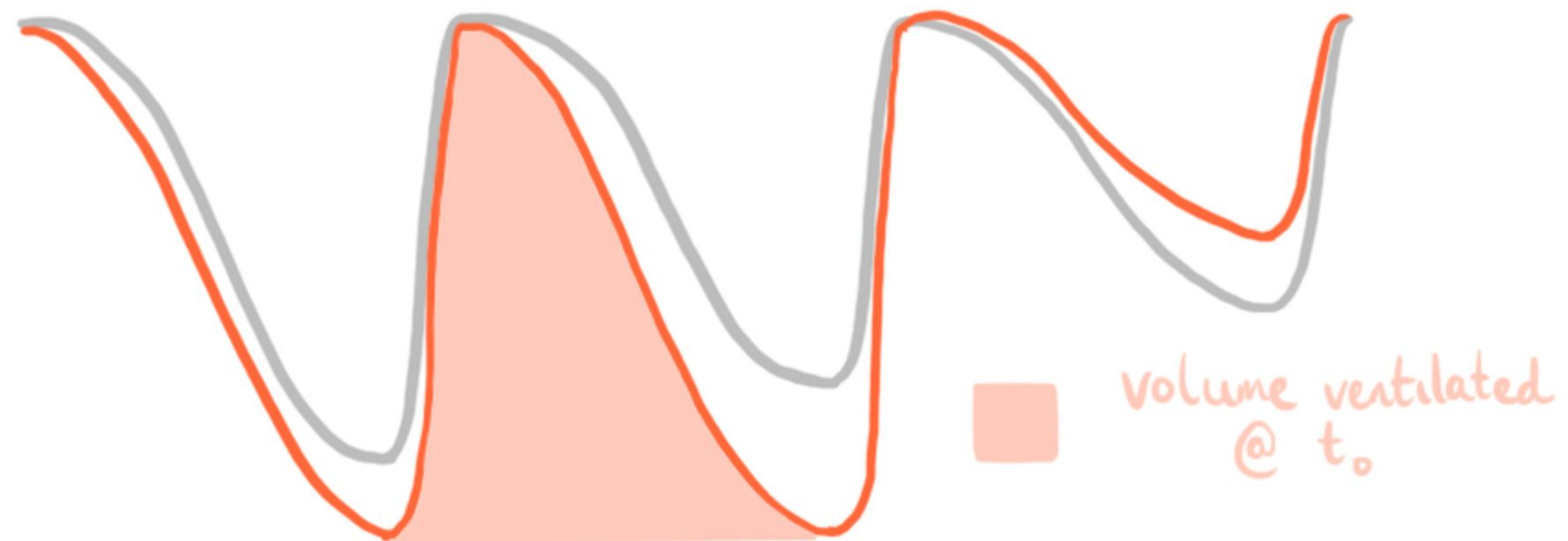
Figure 4.

Forcing (NAO)

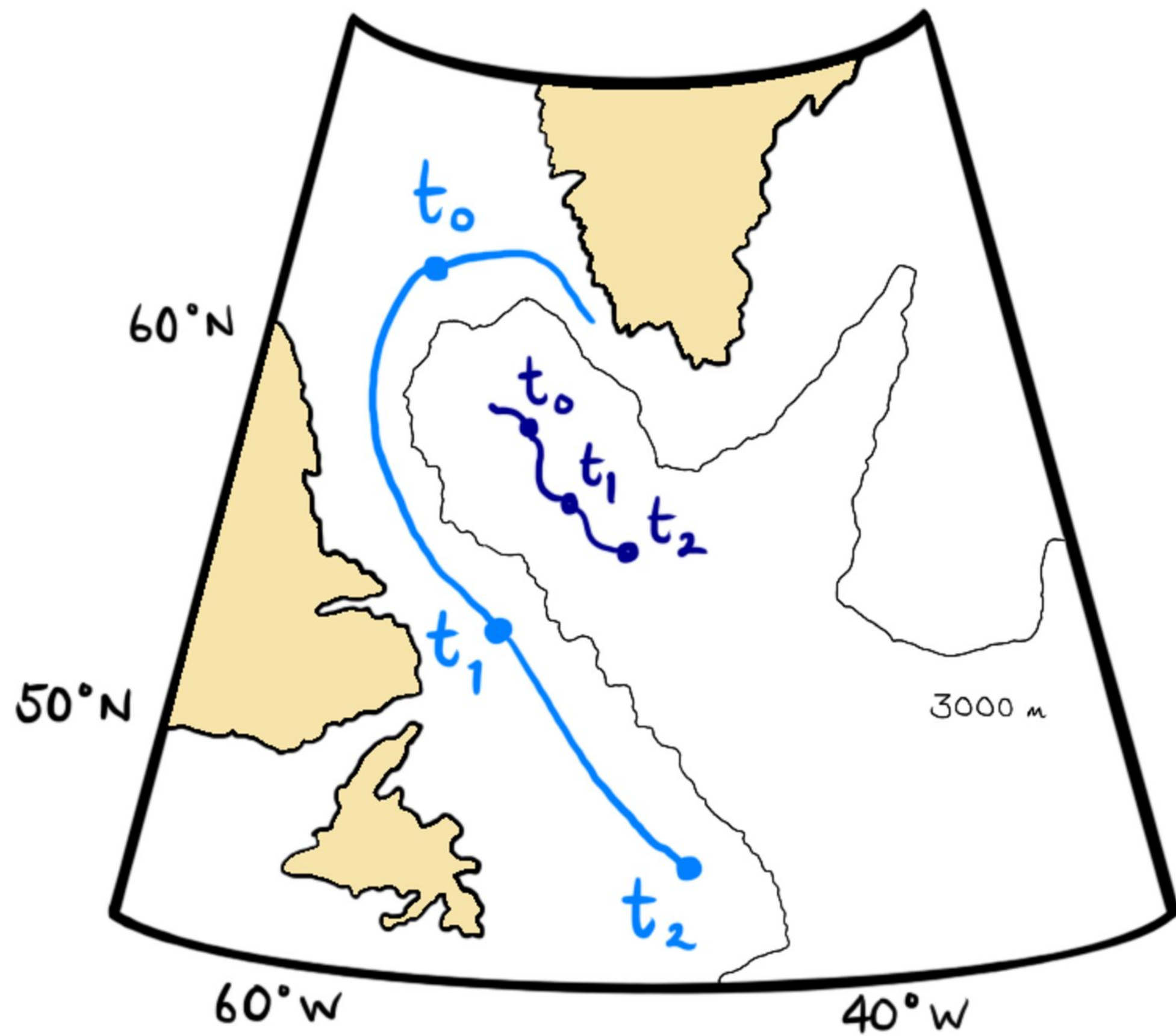
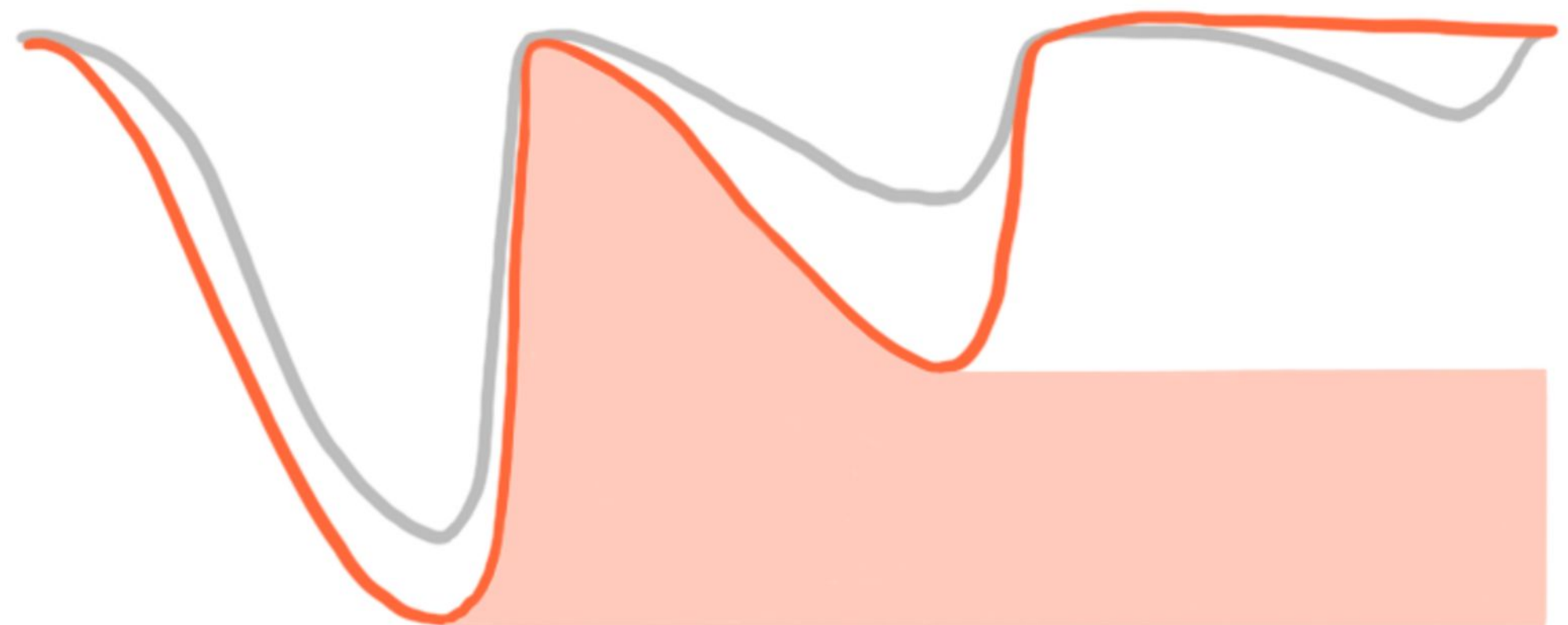


Mixed Layer Depth (following water column)

slow escape (e.g. open ocean)



fast escape (e.g. boundary current)



- slow escape pathway
- fast escape pathway